Batteries & Supercaps

Research Article
doi.org/10.1002/batt.202200335

Chemistry Europe
European Chemical Societies Publishing

www.batteries-supercaps.org

Improved Interface Stability and Zinc-Ions Distribution Achieved by Functional Protective Layer Containing Abundant Oxygen Sites and Regular Channels for Long-Life Zinc-Metal Anodes

Yue Zhang,[a] Tiancun Liu,*[a] Yaling Ji,[a] Jianhua You,[a] Chen Cai,[a] Yi Wen,[a] Zhujun Yao,[a] and Yefeng Yang*[a, b]

Aqueous zinc (Zn)-ion batteries (AZIBs) have attracted much attention for the high safety, economy and nontoxic property, but further practical applications are still hindered due to the severe interfacial corrosion and annoying dendrite growth. Herein, a functional protective layer (FPL) containing abundant oxygen sites and regular channels is proposed as the surface coating to stabilize the Zn-metal anode. Specifically, transferred free water molecules and mitigated Zn-ions can be attracted by these polar oxygen sites, beneficially reliving corrosion behavior, reducing side reactions and inducing uniform Zn deposition. Furthermore, the cross-linked structure with opening channels of FPL benefits electrolyte to quickly arrive the electrode surface and maintain the superior movement of Zn-ions. As a result, a superior cycling performance with high stability of 450 h at 5 mA cm^{-2} and excellent rate behavior have been endowed by Zn electrode loading FPL. In the exploration of practical utilization, full battery consisting of Zn@FPL anode and cathode adopting commercial MnO_2 powder also exhibits an outstanding capacity retention of 98.9% after 300 cycles at 0.5 A g^{-1}. The proposed strategy of constructing a protective layer with functional sites and opening structure shows a good guiding significance for protecting Zn-metal anode.

Introduction

In recent years, due to the vigorous development of portable and wearable electronic products, safe and reliable energy collection and storage systems have dramatically attracted more social attentions. Among many electrochemical energy storage systems, aqueous zinc (Zn)-ion batteries (AZIBs) adopting neutral or medium acid electrolytes are gradually becoming the most promising candidate of the next-generation battery with high safety and nontoxic property. Except for this, aqueous electrolytes used in the AZIBs can reduce the cost of large-scale application and deliver the high ionic conductivity (~1 S cm^{-1}), much superior to these batteries (e.g., lithium-ion and sodium-ion battery) based on organic electrolytes.[1–7] Specifically, as one part of AZIBs, Zn metal anode exhibits some unique characteristics of high theoretical capacity (820 mAh g^{-1}) and low redox potential (−0.76 V compared to a standard hydrogen electrode).[8,9] However, there are some fatal issues, such as dendrites formation, interface corrosion, production of hydrogen evolution and accumulated passivation layer in the Zn metal anode, greatly affecting the effective cycling of Zn electrode and working lifespan of AZIBs.[10,11] Among these mentioned problems, it should be emphatically pointed out that unavoidable generation of Zn dendrites can promote the rapid contact between two electrodes, causing the internal short circuit and cell failure. The large specific surface area produced by generated Zn dendrites with irregular structure may hasten the hydrogen evolution reaction (HER).[12–15] Moreover, uncontrollable growth of inactive Zn metal (dead Zn) derived from the dendritic Zn is inevitable to trigger the poor reversibility of plating/stripping behavior and aggravate the quick deterioration of AZIBs.[16–18] As a result, it is exceedingly significant to effectively inhibit the appearance of Zn dendrites for further enhancing the cycling stability of Zn metal anode and practical application of safe AZIBs.[19–21]

So far, various and effective solutions have been explored by industrious researchers to overcome the dendrite problem and enhance the interface stability.[22–24] Specifically, the gel electrolyte exhibited a positive effect on suppressing the generation of Zn dendrites.[25] In addition, the excellent positive effects have been proved by the strategy of adjusting the electrolyte component and constructing a functional protective layer. Firstly, for the electrolyte modification, various additives including organic and inorganic materials were utilized to relieve the interface corrosion caused by the attack of free water. Typically, the addition of soluble organic component, such as dimethyl sulfoxide,[26] glucose,[27] and ethylene glycol,[28] has been confirmed that the hydrogen bonding between water molecules can be reinforced, which is beneficial to restricting

[a] Y. Zhang, Dr. T. Liu, Y. Ji, J. You, C. Cai, Y. Wen, Dr. Z. Yao, Dr. Y. Yang
School of Materials Science and Engineering
Zhejiang Sci-Tech University
Hangzhou 310018, P. R. China
E-mail: liutc@zstu.edu.cn
yangyf@zstu.edu.cn
[b] Dr. Y. Yang
Institute of Wenzhou
Zhejiang University
Wenzhou 325006, P. R. China

Supporting information for this article is available on the WWW under https://doi.org/10.1002/batt.202200335

the movement of free water and relieving the HER on the electrode surface. In addition, some inorganic components have also taken into consideration for the helpful charge shielding, avoiding the overly concentrated Zn plating and inducing uniformly dispersed Zn deposition.[29,30] However, because of the high electrochemical stability possessed by zinc salts in the aqueous solution, it is generally difficult to produce a solid electrolyte interphase to prevent the direct contact between aqueous electrolyte and Zn electrode, leading to the uncontrollable interfacial side reactions.[31] Moreover, the modification of electrolyte additive may be capable of weakening the ion conduction and reducing the reaction kinetics. Therefore, constructing an artificial protective layer on Zn metal is necessary for stabilizing the electrode interface and suppressing the growth of Zn dendrites.[32,33] Recently, some works have reported that nano-$CaCO_3$ thin layer,[34] ZnF_2 coating[35] and other insulating protective layers prepared by the technology of atomic layer deposition[36] or direct covering[37] can effectively prolong the lifespan and improve cycling stability of Zn metal anode. However, due to the introduction of an additional layer on the Zn electrode, an annoying problem that prepared artificial protective layers usually deliver the sluggish transference of Zn ions may result in the increase of interfacial voltage polarization during the Zn deposition/dissolution process.

Due to the stable structure and porous property, coordination polymer materials have been widely applied in the battery and catalysis research.[38,39] Herein, a functional protective layer (FPL) consisting of synthetic iron (Fe)-based coordination polymer with abundant oxygen (O) sites and polyvinylidene fluoride material is fabricated by a facile method to stabilize the Zn metal anode. Benefiting from the cross-linked structure with opening channels exhibited by FPL, electrolyte is easily able to quickly arrive the electrode surface, maintaining the superior movement rate of Zn ions. Moreover, the electrolyte distribution can be uniformly divided by widely formed opening channels, which promotes the avoidance of locally concentrated behavior of Zn ions and subsequent uniform Zn deposition. The interface stability can be also enhanced by another structural merit of FPL. Due to the existence of abundant polar O sites in Fe-based coordination polymer, there may be homogenous Zn ion distribution caused by the well adsorption and strong interaction between FPL and free water, resulting in the inhibited appearance of Zn dendrites, improved interface stability and reduced side reactions. On the basis of these advantages, the lifespan of AZIBs based on Zn electrode decorated by the FPL can be notably extended. In particular, extremely stable electrochemical performance of symmetric battery consisting of Zn@FPL electrodes has been maintained for 450 h at a high current density of 5 mA cm^{-2} with a large areal capacity of 3 mAh cm^{-2}, displaying the 10 times longer than the device with bare Zn foils. When assembled with commercial MnO_2 powder into the full battery, Zn@FPL electrode shows an extremely stable capacity delivery at 0.5 A g^{-1} for 300 cycles and maintain a high capacity retention of 98.9% in the last cycle as well. The preparation of unique FPL and practical application will help adopt effective strategy to design the Zn metal anode with stable interface and dendrite-free capability for the commercial and economic AZIBs.

Results and Discussion

To stabilize the interface and relive annoying problems of Zn metal anode, a functional protective layer (FPL) with abundant oxygen (O) sites and opening channels has been facilely manufactured to protect Zn electrode. Affected by the unique structure design, constraint on free water and avoidance of concentrated Zn ions flux can be positively improved, which are beneficial to reliving interfacial corrosion, suppressing the appearance of Zn dendrite and further enhancing the electrochemical performances of AZIBs loading Zn metal electrode with FPL (Zn@FPL). As exhibited in Figure 1(a), the detailed process from the initial precursor to the final composite Zn metal electrode can be learned, which mainly contains three parts: the preparation of Fe-based coordination polymer (Fe-NTA), subsequent purification treatment and construction of protected Zn electrode. Initially, Fe-NTA can be produced by a solvothermal method from the reaction solution consisting of $FeCl_3$ source and NTA ligand. After the normal purification treatment, specific amount of Fe-NTA would be uniformly mixed in NMP solvent with PVDF binder at a weight ratio of 4:1 (Fe-NTA vs. PVDF). Finally, the pre-prepared slurry is transferred on Zn foil and made into the FPL using a doctor blade (Figure S1). Figure 1(b and c) shows the morphologies of Fe-NTA material, from which it can be clearly observed the regular fiber with a size about 100–200 nm in diameter.

Figure 1(d and e) displays the SEM images of FPL prepared by Fe-NTA and PVDF, in which fiber-like structure of Fe-NTA and abundant opening channels are noted and there is also a slightly coarse and dense covering, compared to the flat surface of bare Zn foil (Figure S2). In addition, observed from the cross-sectional SEM image (Figure S3), FPL with a thickness about 5 μm can be firmly attached to the Zn surface. Figure 1(f) exhibits the XRD patterns of NTA, Fe-NTA and standard PDF card of $FeCl_3$, respectively, from which some new characteristic peaks have appeared in the result of Fe-NTA, much different from the patterns of NTA and $FeCl_3$. This preliminarily indicates the successful complexation between NTA ligand and Fe^{3+} source. Especially for $FeCl_3$ material, due to the affection of rapid deliquescence, the structure information of sample was not able to be correctly obtained (Figure S4), therefore the corresponding standard PDF card was provided. In particular, some notable peaks (12.1°, 13.4°, 16.6°, 21.8° and 34.4°) in the XRD pattern of Fe-NTA were well accorded with the previous work, strongly manifesting the successful construction of functional Fe-NTA.[40] In addition, the FTIR spectra of NTA powder and Fe-NTA product have been displayed in Figure 1(g). The band ranging from 3100 to 2900 cm^{-1} is assigned to the stretching vibration of C–H. Compared to pure NTA, for Fe-NTA nanowires, the peak at 3043 cm^{-1} becomes very weak because of the coordination of metal ion shifts the stretching vibration peak of C–H bond from 2990 and 2958 cm^{-1} in NTA to 2948 and 2910 cm^{-1}, respectively. It has reported that the chelation

Research Article
doi.org/10.1002/batt.202200335
Chemistry Europe
European Chemical Societies Publishing

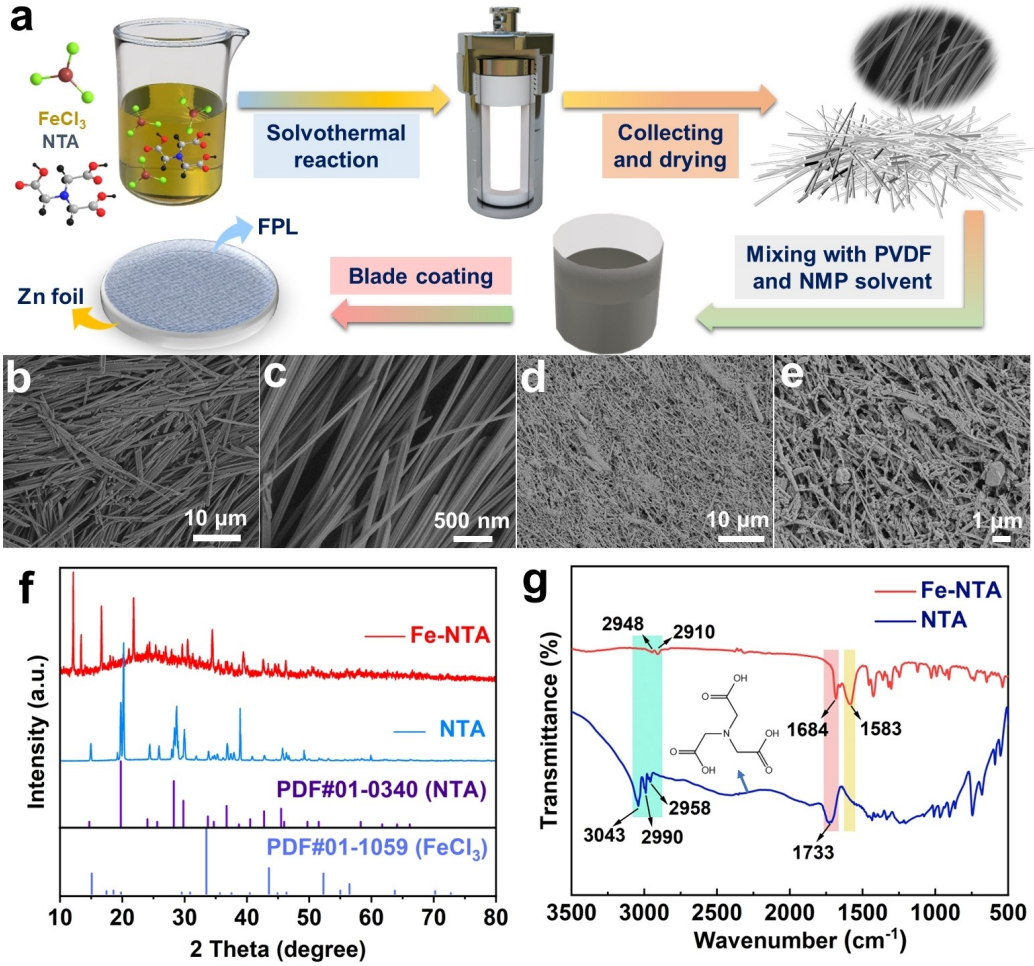

Figure 1. a) Schematic illustration for the fabrication process of Zn@FPL electrode. SEM images at different magnifications of (b and c) Fe-NTA and (d and e) Zn@FPL. f) XRD patterns and g) FTIR spectra of Fe-NTA and NTA powder.

of NTA precursor and metal ion, such as Fe, Ni and Mn, can change the FTIR spectra and exhibit a slight decrease in the C–H frequency, which is different from the pure NTA.[41] The stretching vibration peak of O-containing functional groups of -COOH at 1733 cm^{-1} exhibited in NTA has spitted into two small peaks located at 1684 and 1583 cm^{-1} in Fe-NTA, which can be attributed to the coordination between Fe ions and C=O band, causing the new formation of –COOFe coordination group.[42] Specifically, these abundant O polar sites are able to greatly adsorb Zn ions and induce uniform distribution, causing dispersed Zn deposition and inhibited generation of dendritic Zn.

Figure 2(a and b) shows the results of contact angle between 2 M $ZnSO_4$ and bare Zn or Zn@FPL electrode, from which a small contact angle of 91.56° and good wettability have been delivered by Zn@FPL, possibly resulting from abundant polar O sites and enhanced interaction with water molecules. However, there was a high value of 106.09° on the bare Zn foil, further indicating the poor interfacial hydrophilicity and zincophilicity. In order to study the role of FPL in improving Zn electrode, Tafel tests have been carried out, as shown in Figure 2(c). There was a corrosion potential of 0.001 V for Zn@FPL, higher than the corrosion performance of −0.006 V for bare Zn. The increase of potential demonstrates the effective improvement for interfacial corrosion due to the modification of FPL on Zn foil. Moreover, the immersion test was conducted in the electrolyte of 2 M $ZnSO_4$ for further examining the practical feedback. As displayed in Figure 2(d and e), SEM images of bare Zn and Zn@FPL electrode show a little notable morphology difference after the immersion of 7 days. Interestingly, although encountering some influences of electrolyte, electrode surface of Zn@FPL after removing the protective layer still maintained the comparatively flat state with slight wrinkle, which should be the by-product of $Zn_4SO_4(OH)_6 \cdot 3H_2O$. These by-products with poor transference of Zn ions would be generated on the corrosion process due to the local pH elevation caused by competitive HER.[43] In contrast with Zn@FPL, it could be evidently viewed that numerous blocks (by-product) were unevenly dispersed on the bare Zn, indicating the relatively concentrated distribution of Zn ions and more severe interfacial corrosion. The structure information of electrodes after the immersion procedure was also determined. Figure 2(f) shows the XRD results of Zn and Zn@FPL electrode immersed for 7 days, in which some characteristic

Research Article
doi.org/10.1002/batt.202200335
Chemistry Europe
European Chemical Societies Publishing

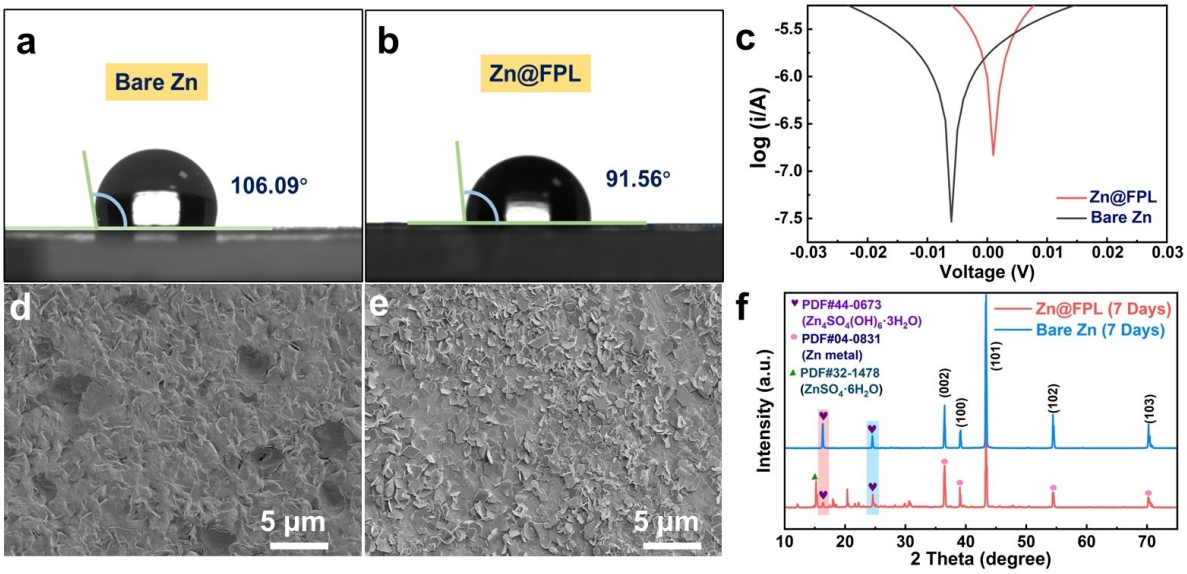

Figure 2. Contact angles of electrolyte on a) the bare Zn and b) Zn@FPL. c) Tafel polarization curves for bare Zn and Zn@FPL electrodes. SEM images of d) bare Zn and e) Zn@FPL electrodes immersed in 2 M $ZnSO_4$ after 7 days. f) Related XRD patterns of electrodes after the immersion of 7 days.

peaks located at 16.3° and 24.5° were the by-product of $Zn_4SO_4(OH)_6 \cdot 3H_2O$ (PDF#44-0673) and another five peaks at 39.3°, 70.7°, 43.2°, 54.3°, 70.1° and 70.7° should be Zn metal (PDF#04-0831). This manifests that both electrodes are not able to avoid the corrosion influence because of the incomplete isolation with electrolyte. In particular, the peak intensities of by-product on bare Zn seem much higher than those on Zn@FPL, well determining that more serious interfacial corrosion and by-product accumulation on Zn foil without any protection. It should be noted that a distinct diffraction peak around 15° should be attributed to residual $ZnSO_4 \cdot 6H_2O$ (PDF#32-1478) due the incomplete cleaning during preparing sample. In addition, due to the preservation of FPL, corresponding signals could be also detected and exhibited by other unmarked peaks between 10° and 30° in the pattern of Zn@FPL electrode. To further explore the effective ability of FPL, XRD patterns of Zn and Zn@FPL electrode after the immersion of 14 days were also displayed in Figure S5. Notably, peak intensities of two electrodes all have been enhanced because of the continuation of corrosion, compared to the results in Figure 2(c). But the anti-corrosion effect of Zn@FPL electrode was still superior to bare Zn foil.

To determine the ability of abundant O sites in inducing Zn ion distribution, Figure 3(a) shows Chronoamperometry curves of Zn and Zn@FPL electrodes operated at an overpotential of −0.15 V for 350 s, in which the current variation with time can reflect the Zn nucleation behavior. Briefly, after the two-dimensional diffusion process with a short time of 50 s, a stable three-dimensional transport process could be started on the Zn@FPL electrode, indicating the homogeneous Zn stripping/plating behavior. On the contrary, for bare Zn, there was a continuous current increase for a long time of 350 s, which represented a slow two-dimensional diffusion performance and a rougher deposition behavior. The difference of Zn nucleation on Zn and Zn@FPL electrodes can be exhibited in Figure 3(b). Specifically, dendritic Zn metal is more inclined to developing on the surface of bare Zn due to the poor performance of two-dimensional diffusion. However, quick 2D diffusion of Zn ions on Zn@FPL is beneficial to dispersing on the larger surface and producing more nucleation sites, effectively avoiding the concentrated deposition and growth of Zn metal. The optimized diffusion behavior should be explained by abundant O sites in FPL, which can effectively adsorb Zn ions and quickly distribute them.

In order to verify the superior ability of stabilizing Zn metal, SEM images of Zn and Zn@FPL electrodes cycled at 1 mA cm^{-2} with 1 mAh cm^{-2} in symmetric cells have been provided and shown some obvious differences. It should be specially pointed out that the morphology examinations were conducted on the working electrodes loading plated Zn of 1 mAh cm^{-2}. As shown in Figure 3(c), for Zn@FPL, there were some flakes on the Zn electrode without the FPL after 10 cycles. Even cycled after 50 cycles, flat and dense Zn flakes were also observed (Figure 3d), manifesting the excellent effect of uniformly guiding Zn deposition. The stability performance of the covered FPL after continuous cycling has also been examined and displayed in the Figure S6, from which the morphology of the protective layer after 50 cycles could still show similar to that of pristine Zn@FPL in Figure 1(d—e), manifesting the superior stability of this functional layer. Especially, as shown in Figure S7, related XRD patterns at 5°–15° of Fe-NTA, Zn@FPL and cycled electrode were also obtained. The peak at 8.1° should be $Zn_4SO_4(OH)_6 \cdot 3H_2O$ and other two peaks at 6.9° and 12.1° were attributed to the Fe-NTA, well corresponded with the peaks in the Fe-NTA and Zn@FPL. The clear comparison further indicates the excellent structural stability of Fe-NTA material with Fe ion. However, as displayed in Figure 3(e), few large protuberances of plated Zn were on the surface of bare Zn and inhomoge-

Research Article
doi.org/10.1002/batt.202200335
Chemistry Europe
European Chemical Societies Publishing

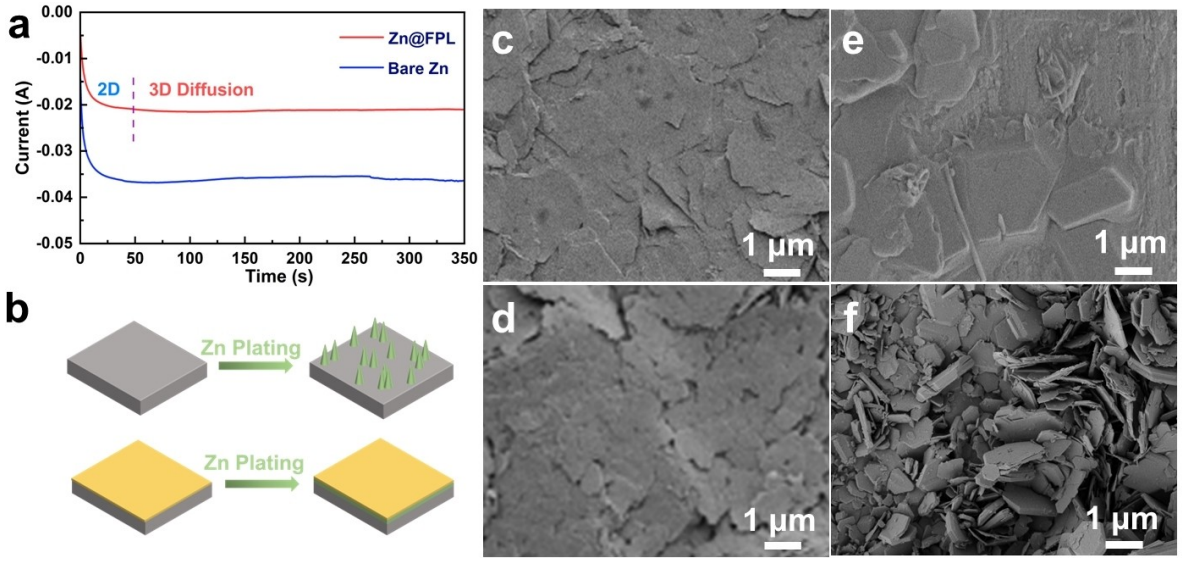

Figure 3. a) Chronoamperometry curves conducted at a potential of −0.15 V. b) Schematic diagram of the surface morphology changes of bare Zn and Zn@FPL during the Zn plating process. SEM images of Zn@FPL after c) 10 and d) 50 cycles. SEM images of bare Zn after e) 10 and f) 50 cycles. The test condition is controlled at 1 mA cm^{-2} with Zn striping/plating time of 1 h for each cycle.

neous distribution could be noticed as well, which may be caused by the inferior capability of decentralizing Zn ions. As the cycling continues to 50 cycles (Figure 3f), more worse surface situation has happened on the bare Zn, in which numerous irregular Zn bulks and dendrites generated and notable interfacial gaps resulting from the severe corrosion of unavoidable HER also appeared. As a result, the excellent performance of abundant O sites of FPL in promoting dendrite-free behavior is able to be learned by comparation with bare Zn, and this will be definitely to improve the electrochemical results of AZIBs.

Related electrochemical performances were also measured by symmetric cells to further explore the positive effects of FPL modification. Figure 4(a) exhibits the EIS results of cells with bare Zn and Zn@FPL, from which Zn@FPL delivers a similar interface resistance about 2 Ω due to the opening structure. In

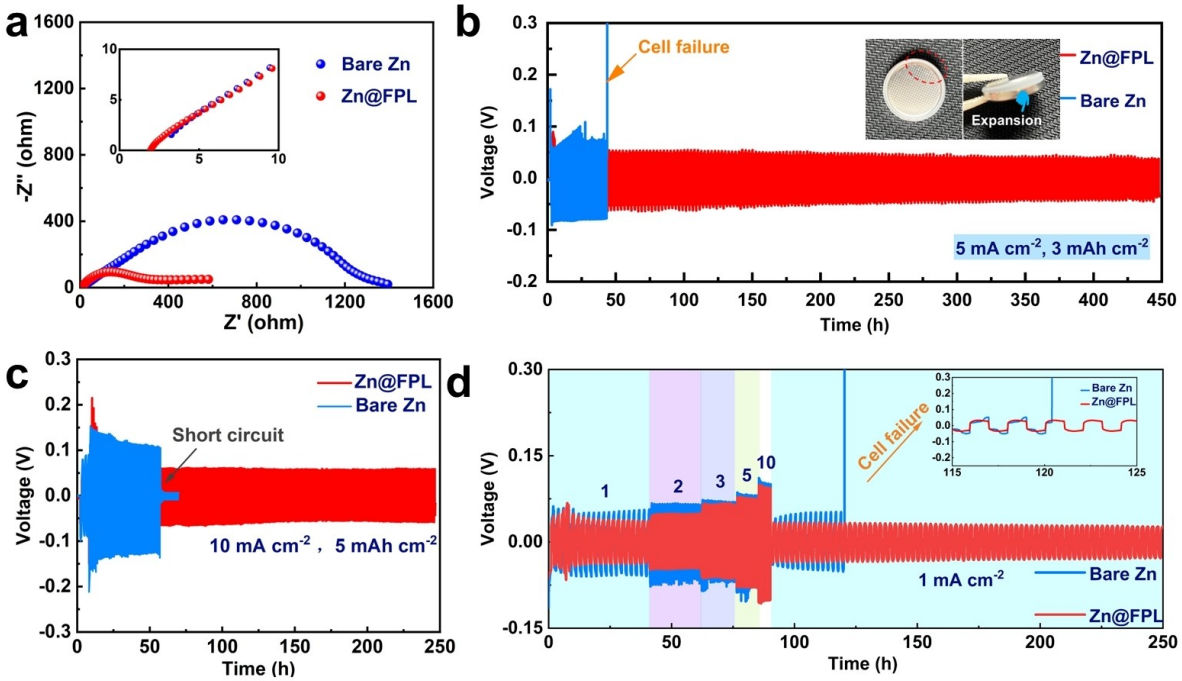

Figure 4. a) Nyquist plots of bare Zn and Zn@FPL. Typical voltage profiles of symmetric cells at b) 5 mA cm^{-2}, 3 mAh cm^{-2} and c) 10 mA cm^{-2}, 5 mAh cm^{-2}. d) Rate performances of cells with bare Zn and Zn@FPL.

Research Article
doi.org/10.1002/batt.202200335
Chemistry Europe
European Chemical Societies Publishing

addition, charge transfer impedance of Zn@FPL (300 Ω) was significantly smaller than that of bare Zn (1200 Ω), implying the enhanced reaction kinetics and reduced interfacial polarization. For determining the effective FPL in prolonging the working lifespan of Zn metal electrode, long-term cycling results of symmetric cells based on bare Zn and Zn@FPL have been carried out. As displayed in Figure S8, a superior cycling lifetime of 550 h could be provided by the cell with Zn@FPL, when worked at 3 mA cm^{-2} with the plating/stripping capacity of 1 mAh cm^{-2}. In sharp contrast, there was extremely short performance of 110 h for the bare Zn-based cell, and then a notable internal short circuit occurred. As the test condition changed to a higher current density of 5 mA cm^{-2} (Figure 4b), a greatly stable state with low voltage polarizations was able to be maintained by the cell loading Zn@FPL for 450 h, 10 times longer than the time of Zn|Zn cell (45 h). Moreover, compared to Zn@FPL-based cell, interfacial polarization of Zn|Zn cell was actually larger, which should be mainly resulted from more severer side reactions (HER and by-product formation) on the electrode interface. In particular, due to the HER, hydrogen has been gradually accumulated and finally resulted in the bulge and dehiscence of coin cell (cycling failure), which was proved by the failed coin cell (inserted optical images). However, because of the excellent guidance of Zn ions and improved interface stability, durable cycling performance could extend to 450 h and the development of Zn dendrites was effectively suppressed as well. Similarly, working performances of two cells have also been conducted at higher current density (10 mA cm^{-2}) and larger cycling capacity (5 mAh cm^{-2}), as shown in Figure 4(c). Expectedly, stable cycling plots with low interfacial polarization and comparatively durable lifetime of 240 h could still be delivered by Zn@FPL-based cell. In contrast, poor cycling behavior and even rapid internal short circuit were exhibited by Zn|Zn cell, although being stabilized at a mild test condition of 0.5 mA cm^{-2} for 10 cycles. The positive effects of reducing the production of Zn dendrites and reliving electrode interface given by the FPL could also be confirmed by the rate performance (Figure 4d). From 1 to 10 mA cm^{-2}, it was able to observe a flat cycling and low voltage polarization of symmetric cell with Zn@FPL in the whole rate process of 250 h. But Zn|Zn cell rapidly encountered a cell failure after returning to 1 mA cm^{-2}, in addition to the high interface polarization. Based on the measured result comparation, the modification of FPL has been further proved the enhanced abilities of prolonging the lifespan, improving the interface stability and reliving the concentrated Zn growth of AZIBs.

To explore the possibility of practical application, Zn@FPL anode, MnO_2 cathode and electrolyte of 2 M $ZnSO_4$ with 0.1 M $MnSO_4$ additive were together assembled into aqueous full battery (AFB). It should be specially mentioned that the cathode was prepared by the commercial MnO_2 powder. As exhibited in the diagrammatic sketch of Figure 5(a), the assembled AFB was mainly composed of six parts: anode, cathode, separator, electrolyte and external packing cases. As shown in Figure 5(b), SEM image of MnO_2 has been also obtained, obviously displaying the large-bulk and irregular morphology. The large size of cathode material is definitely to weaken the material activation and full release of capacity. Figure 5(c) performs the XRD pattern of purchased MnO_2 material, from which three typical peaks located at should be plane 100, 101 and 102, exactly accorded with the standard card (PDF#30-0820). Notably, a strong peak at 22.0° should be provided by another kind of MnO_2 with different crystal structure (PDF#44-0142) and correspondingly attributed to plane 101. In Figure 5(d), long-term charge/discharge process of AFB adopting bare Zn and Zn@FPL anode have been

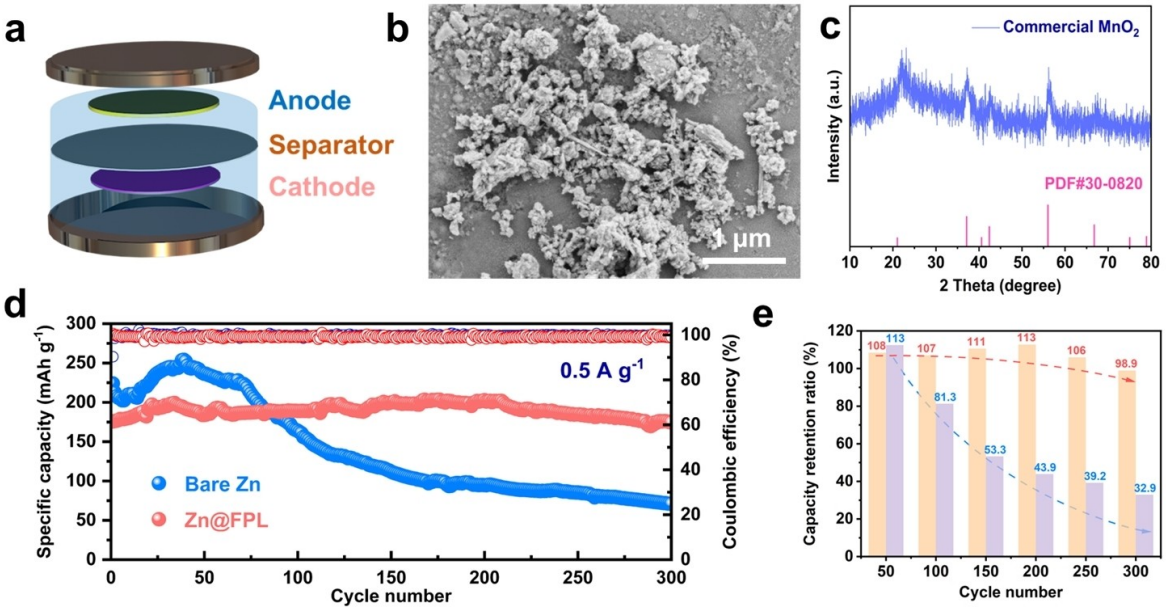

Figure 5. a) Schematic diagram of the assembled full cell. b) SEM image and c) XRD result of commercial MnO_2 powder. d) Electrochemical performance of MnO_2-based cells adopting bare Zn and Zn@FPL electrode. e) The comparison about capacity retention of full batteries with bare Zn and Zn@FPL electrode during the whole 300 cycles.

Research Article
doi.org/10.1002/batt.202200335

measured at the test requirement of 0.5 A g^{-1} as well. Specifically, an excellent initial specific capacity of 176.2 mAh g^{-1} and high capacity delivery of 174.4 mAh g^{-1} even after 300 cycles could be performed by Zn@FPL-based AFB. Moreover, there was always a stable cycling state during the whole 300 cycles and an ultra-high capacity retention of 98.9% after the 300th cycle, which indicated the effective inhibition of side reactions containing water consumption, loss of $ZnSO_4$ in electrolyte, and generation of dendritic Zn. In contrast, superior capacity performance over 200 mAh g^{-1} in the first 50 cycles for AFB with bare Zn was much better than Zn@FPL at the same condition, but a rapid capacity decay appeared, which may be resulted from the excessive loss of active $ZnSO_4$ caused by the formation of passivation layer, dissolution of MnO_2 and consumption of free water due to the hydrogen production. Affected by these problems, a low capacity of 73.7 mAh g^{-1} and capacity retention of 32.9% (224.1 mAh g^{-1} at 1st cycle) were determined after 300 cycles respectively. Similarly, the superior capacity retention of the AFB with Zn@FPL electrode could be well determined by the charge and discharge curves at different cycles, as provided in Figure S9. It can be also predicted that complicated issues of interfacial side reactions will bring out the decline of reaction kinetics and mass transfer. As shown in Figure 5(e), a comparison chart about capacity retention ratio of different AFBs has been provided. Because of inevitable side reactions, bare Zn-based cell delivered a continuous decrease from the high value of 113% at 50th cycle to 32.9% at the last 300th cycle. On the contrary, AFB with Zn@FPL anode could always maintain superior retention ratios nearly 100%, further manifesting the effective protection of FPL for Zn metal anode.

Based on the aforementioned results and discussion, it is necessary to visually make clear that different interfacial behaviors happen on bare Zn and Zn@FPL electrode, as shown in the schematic diagram of Zn plating/stripping process of Figure 6. As Zn deposition starts, mitigated Zn ions and free water molecules are preferred to be attracted by massive polar O sites in the decoration interface of FPL, in which abundant −COOH groups may play an important role. Benefiting from the generated uniform distribution of Zn ions and excellent activity suppression of free water molecules, both dendrite-free situation of Zn plating/stripping and improved ability of interfacial anti-corrosion are achieved on Zn@FPL electrode, which have been determined from related results of anti-corrosion test (Figure 2c–f) and obtained SEM images of checking the surface morphology of cycled Zn@FPL (Figure 3c and d). However, it should be understood that the opening structure provided by FPL is unable to completely avoid these annoying side reactions, such as the formation of passion layer (Figure S5) and generated H_2 release in small amount because of direct contact with electrolyte. In contrast, without any protection, severe interfacial corrosion (Figure 2e) and inhomogeneous Zn deposition/dissolution behavior (Figure 3e and f) occur on bare Zn. Moreover, there is a bad HER and a large amount of H_2 generation (inset in Figure 4b). Through the comparison in electrochemical performances, prolonged cycling lifespan (Figure 4b–d) and slow capacity decay (Figure 5d)

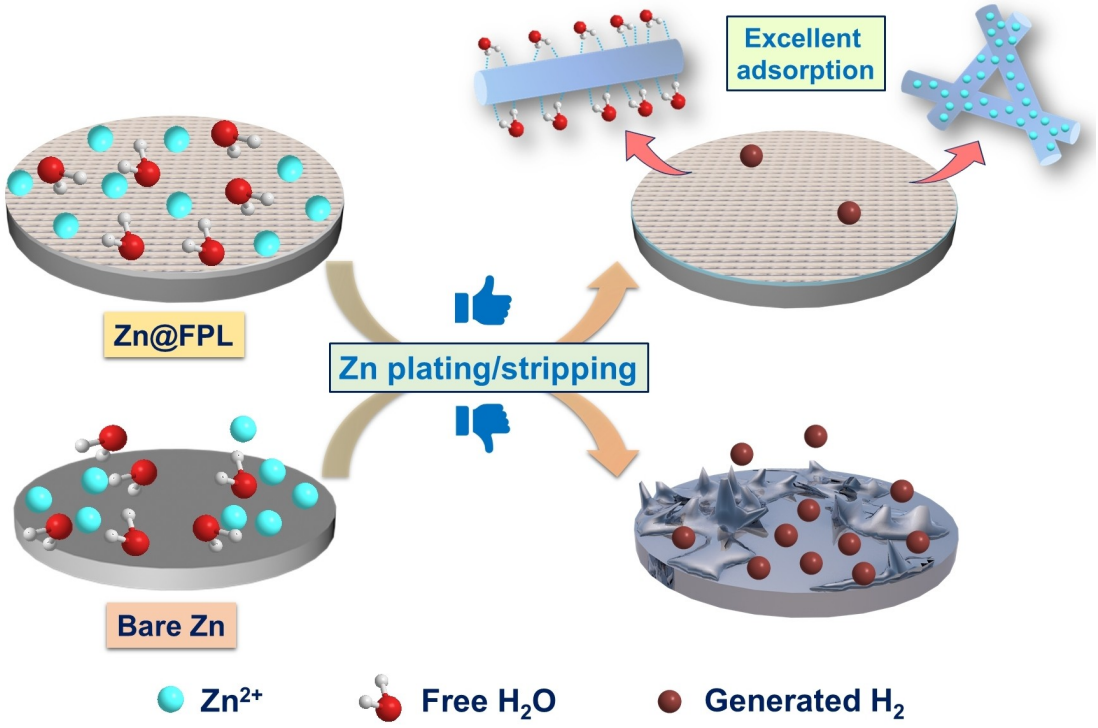

Figure 6. Schematic diagram of the behavior comparison between bare Zn and Zn@FPL electrode during the Zn deposition process, and different ability of reliving the interfacial side reactions.

performed by Zn@FPL can further indicate the significance of FPL and necessity of protective treatment on Zn metal anode.

Conclusion

Briefly, a functional protective layer (FPL) containing abundant O sites and opening structure has been proposed to stabilize Zn metal electrode for enhancing the electrochemical performances of aqueous Zn ion batteries. Benefiting from the excellent adsorption with free water and uniform distribution of Zn ions offered by O sites, improved anti-corrosion, avoided situation of concentrated Zn deposition and prolonged cycling lifespan can be performed by Zn@FPL electrode. In the electrochemical tests, the symmetric battery adopting Zn@FPL stably achieves an excellent rate capability and a durable performance of 450 h at 5 mA cm^{-2} with 3 mAh cm^{-2}, 10 times longer than Zn-based cell. Moreover, when assembled with commercial MnO_2 material, Zn@FPL anode also performs a stable capacity delivery over 174.4 mAh g^{-1} for 300 cycles and slow average capacity decay of 1.1% per cycle at 0.5 A g^{-1}. This selection of effective protective layer and successful application in Zn metal anode will positively extend the possibility of realizing the large-scale utilization of practical AZIBs.

Experimental Section

Raw materials: Iron chloride ($FeCl_3$, $\geq$99.9% of high purity), nitrilotriacetic acid (NTA, $\geq$99.0% of purity), Polyvinylidene fluoride (PVDF) binder, N-methyl pyrrolidone (NMP) solvent were all purchased from Aladdin. Isopropanol solvent and MnO_2 powder were obtained from Sinopharm Chemical Reagent Co. All chemicals were used directly without further purification.

Fabrication of Fe-based coordination polymer and modified Zn electrode: In a typical synthesis process. Fe-based coordination polymer, noted as Fe-NTA, was prepared by a facile solvothermal reaction. Firstly, a fixed amount of $FeCl_3$ (2.1 mmol, 0.34 g) was dissolved into a mixed solution of isopropanol (30 mL) and distilled water (30 mL). Subsequently, prepared NTA (6.3 mmol, 1.20 g) powder was added into the former solution. After stirring for 30 min, the mixture was then transferred into a Teflon lined autoclave and treated at 180 °C for 24 h. When the reaction finished and the autoclave's state cooled down into room temperature, the product (Fe-NTA) was collected, purified with excessive amount of distilled water and ethanol, and then dried at 60 °C for 12 h in a vacuum oven. For the preparation of Fe-NTA modified Zn electrode, a mixture containing Fe-NTA and PVDF at a weight ratio of 4:1 should be firstly obtained and evenly dispersed in NMP solvent to obtain a uniform slurry. Afterwards, the slurry was coated on the Zn foil by a film scraper.

Material characterization: The surface morphologies of Fe-NTA and electrodes after cycling were examined via scanning electron microscopy (SEM, Zeiss Ultra 55). X-ray diffraction (XRD) studies were conducted on an X-ray diffractometer (Bruker D-8 Advance) with Cu Kα radiation. The Fourier Transform Infrared Spectroscopy (FTIR) was measured on Bruker TENSOR 27. The studies of surface wettability of various substrates to the electrolyte were performed by the Dataphysics OCA20.

Electrochemical measurements: All the electrochemical performance tests were performed by assembled CR2032 coin cells in a Neware battery system at room temperature. The CR2032 coin cells were installed in the air and composed of an electrolyte of 2 M $ZnSO_4$, glass fiber as the separator and selected electrode. The electrochemical impedance spectroscopy (EIS) curves, chronoamperometry (CA) and Tafel were conducted on a CHI760E electrochemical workstation. In particular, for the assembly of aqueous full batteries, the used cathode was made by blending commercial MnO_2 powder, Super P, and PVDF binder with a weight ratio of 7:2:1 in NMP solvent. And the as-formed uniform slurry was casted onto stainless steel foils. Compared to the asymmetric and symmetric cell, different electrolyte of 2 M $ZnSO_4$ with 0.1 M $MnSO_4$ (additive) aqueous solution was adopted. Finally, all full batteries were tested between 0.8 V and 1.9 V.

Supporting information

The Supporting Information can be obtained free of charge at Royal Society of Chemistry website.

Acknowledgements

This work is well supported by the Zhejiang Provincial Natural Science Foundation of China (No. LY21E020010), Scientific Fundamental Fund of Zhejiang Sci-Tech University (Grant No. 21212304-Y, 2021Y005 and 20212297-Y) and National Natural Science Foundation of China (No. 52102315).

Conflict of Interest

The authors declare no competing financial interest.

Data Availability Statement

The data that supports the findings of this study are available in the supplementary material of this article.

Keywords: hydrogen evolution reaction · interfacial protection · ion redistribution · Zn dendrite · Zn metal anode

[1] C. Yang, H. Xie, W. Ping, K. Fu, B. Liu, J. Rao, J. Dai, C. Wang, G. Pastel, L. Hu, *Adv. Mater.* **2019**, *31*, 1804815.
[2] J. Cao, D. Zhang, X. Zhang, Z. Zeng, J. Qin, Y. Huang, *Energy Environ. Sci.* **2022**, *15*, 499–528.
[3] Z. Liu, L. Qin, B. Lu, X. Wen, S. Liang, J. Zhou, *ChemSusChem* **2022**, *15*, e202200348.
[4] J. Cui, Z. Guo, J. Yi, X. Liu, K. Wu, P. Liang, Q. Li, Y. Liu, Y. Wang, Y. Xia, J. Zhang, *ChemSusChem* **2020**, *13*, 2160–2185.
[5] X. Li, Z. Chen, Y. Yang, S. Liang, B. Lu, J. Zhou, *Inorg. Chem. Front.* **2022**, *9*, 3986.
[6] D. Gueon, T. Kim, J. Lee, J. H. Moon, *Nano Energy* **2022**, *95*, 106980.
[7] Z. Liu, Y. Yang, S. Liang, B. Lu, J. Zhou, *Small Struct.* **2021**, *2*, 2100119.
[8] Y. An, Y. Tian, K. Zhang, Y. Liu, C. Liu, S. Xiong, J. Feng, Y. Qian, *Adv. Funct. Mater.* **2021**, *31*, 2101886.
[9] Y. Tang, C. Liu, H. Zhu, X. Xie, J. Gao, C. Deng, M. Han, S. Liang, J. Zhou, *Energy Storage Mater.* **2020**, *27*, 109–116.

[10] C. Xu, B. Li, H. Du, F. Kang, *Angew. Chem. Int. Ed.* **2012**, *51*, 933–935; *Angew. Chem.* **2012**, *124*, 957–959.
[11] J. Hao, X. Li, X. Zeng, D. Li, J. Mao, Z. Guo, *Energy Environ. Sci.* **2020**, *13*, 3917–3949.
[12] W. Du, E. Ang, Y. Yang, Y. Zhang, M. Ye, C. Li, *Energy Environ. Sci.* **2020**, *13*, 3330–3360.
[13] H. Jia, Z. Wang, B. Tawiah, Y. Wang, C.-Y Chan, B. Fei, F. Pan, *Nano Energy* **2020**, *70*, 104523.
[14] S. Bhoyate, S. Mhin, J.-e. Jeon, K. Park, J. Kim, W. Choi, *ACS Appl. Mater. Interfaces* **2020**, *12*, 27249–27257.
[15] H. Li, L. Ma, C. Han, Z. Wang, Z. Liu, Z. Tang, C. Zhi, *Nano Energy* **2019**, *62*, 550–587.
[16] J. Zhao, J. Zhang, W. Yang, B. Chen, Z. Zhao, H. Qiu, S. Dong, X. Zhou, G. Cui, L. Chen, *Nano Energy* **2019**, *57*, 625–634.
[17] N. Guo, W. Huo, X. Dong, Z. Sun, Y. Lu, X. Wu, L. Dai, L. Wang, H. Lin, H. Liu, H. Liang, Z. He, Q. Zhang, *Small Methods* **2022**, 2200597.
[18] D. Yuan, W. Manalastas, L. Zhang, J. Chan, S. Meng, Y. Chen, M. Srinivasan, *ChemSusChem* **2019**, *12*, 4889–4900.
[19] L. Zhou, F. Yang, S. Zeng, X. Gao, X. Liu, X. Cao, P. Yu, X. Lu, *Adv. Funct. Mater.* **2021**, *32*, 2110829.
[20] S. Pu, C. Gong, Y. Tang, Z. Ning, J. Liu, S. Zhang, Y. Yuan, D. Melvin, S. Yang, L. Pi, J. Marie, B. Hu, M. Jenkins, Z. Li, B. Liu, S. Tsang, T. Marrow, R. Reed, X. Gao, P. Bruce, A. Robertson, *Adv. Mater.* **2022**, 2202552.
[21] Y. Liu, T. Guo, Q. Liu, F. Xiong, M. Huang, Y. An, J. Wang, Q. An, C. Liu, L. Mai, *Mater. Today* **2022**, *28*, 10056.
[22] C. Li, X. Xie, S. Liang, J. Zhou, *Energy Environ. Mater.* **2020**, *3*, 146–159.
[23] T. Liu, J. Hong, J. Wang, Y. Xu, Y. Wang, *Energy Storage Mater.* **2022**, *45*, 1074–1083.
[24] C. Deng, X. Xie, J. Han, Y. Tang, J. Gao, C. Liu, X. Shi, J. Zhou, S. Liang, *Adv. Funct. Mater.* **2020**, *30*, 202000599.
[25] B. Zhang, L. Qin, Y. Fang, Y. Chai, X. Xie, B. Lu, S. Liang, J. Zhou, *Sci. Bull.* **2022**, *67*, 955.
[26] Q. Nian, X. Zhang, Y. Feng, S. Liu, T. Sun, S. Zheng, X. Ren, Z. Tao, D. Zhang, J. Chen, *ACS Energy Lett.* **2021**, *6*, 2174–2180.
[27] P. Sun, L. Ma, W. Zhou, M. Qiu, Z. Wang, D. Chao, W. Mai, *Angew. Chem. Int. Ed.* **2021**, *60*, 18247–18255.
[28] N. Wang, Y. Yang, X. Qiu, L. Dong, G. Wang, Y. Xia, *ChemSusChem* **2020**, *13*, 5556–5564.
[29] X. Guo, Z. Zhang, J. Li, N. Luo, G.-L. Chai, T. Miller, F. Lai, P. Shearing, D. Brett, D. Han, Z. Weng, G. He, I. Parkin, *ACS Energy Lett.* **2021**, *6*, 395–403.
[30] T. Sun, S. Zheng, H. Du, Z. Tao, *Nano-Micro Lett.* **2021**, *13*, 204.
[31] M. Li, Z. Li, X. Wang, J. Meng, X. Liu, B. Wu, C. Han, L. Mai, *Energy Environ. Sci.* **2021**, *14*, 3796–3839.
[32] H. He, H. Qin, J. Wu, X. Chen, R. Huang, F. Shen, Z. Wu, G. Chen, S. Yin, J. Liu, *Energy Storage Mater.* **2021**, *43*, 317–336.
[33] Y. An, Y. Tian, C. Liu, S. Xiong, J. Feng, Y. Qian, *ACS Nano* **2021**, *15*, 15259–15273.
[34] L. Kang, M. Cui, F. Jiang, Y. Gao, H. Luo, J. Liu, W. Liang, C. Zhi, *Adv. Energy Mater.* **2018**, *8*, 1801090.
[35] Y. Yang, C. Liu, Z. Lv, H. Yang, Y. Zhang, M. Ye, L. Chen, J. Zhao, C. Li, *Adv. Mater.* **2021**, *33*, 2007388.
[36] Z. Zeng, Y. Zeng, L. Sun, H. Mi, L. Deng, P. Zhang, X. Ren, Y. Li, *Nanoscale* **2021**, *13*, 12223–12232.
[37] U. Khan, A. Nairan, J. Gao, Q. Zhang, *Small Structures* **2022**, DOI: 10.1002/sstr.202200109.
[38] T. Zhao, H. Wu, X. Wen, J. Zhang, H. Tang, Y. Deng, S. Liao, X. Tian, *Coord. Chem. Rev.* **2022**, *468*, 214642.
[39] N. Wang, M. Zhang, L. Liu, J. Zheng, J. Xu, T. Hayat, N. S. Alharbi, *Nanotechnology* **2019**, *30*, 415602.
[40] X. Chen, W. Li, S. Hu, N. Akhmedov, D. Reed, X. Li, X. Liu, *Nano Energy* **2022**, *98*, 107269.
[41] F. J. M. Rajabalee, *Spectrochim. Acta* **1974**, *30 A*, 891.
[42] H. Li, R. Xu, Y. Wang, B. Qian, L. Chen, H. Jiang, Y. Yang, Y. Xu, *RSC Adv.* **2014**, *4*, 51960–51965.
[43] X. Zhang, J. Hu, N. Fu, W. Zhou, B. Liu, Q. Deng, X. Wu, *InfoMat.* **2022**, e12306.

Manuscript received: July 29, 2022
Revised manuscript received: August 25, 2022
Accepted manuscript online: August 29, 2022
Version of record online: September 12, 2022